Journal of Alloys and Compounds 509 (2011) 114–122

Contents lists available at ScienceDirect

Journal of Alloys and Compounds

journal homepage: www.elsevier.com/locate/jallcom

Effects of ultrasonic treatment on microstructure and tensile strength of AZ91 magnesium alloy

M. Khosro Aghayani, B. Niroumand*

Department of Materials Engineering, Isfahan University of Technology, Isfahan 84156-83111, Iran

ARTICLE INFO

Article history:
Received 6 January 2010
Received in revised form 25 August 2010
Accepted 27 August 2010
Available online 6 September 2010

Keywords:
Ultrasonic treatment
Metals and alloys
AZ91 magnesium alloy
Microstructure
Intermetallic phase
Tensile strength

ABSTRACT

In this study, the effects of ultrasonic treatment on microstructural features and tensile strength of AZ91 magnesium alloy were investigated. AZ91 melts were subjected to ultrasonic waves of different power levels for 5 min using an ultrasonic device with frequency of about 20 kHz and maximum power of 600 W and cast in sand moulds. The results showed that ultrasonic treatment of the melt prior to casting had a significant effect on the size and sphericity of α-Mg dendrites as well as on the size, continuity, sphericity and distribution of intermetallic particles formed during cooling and solidification of the alloy. Increasing the applied ultrasonic power resulted in smaller, more rounded and better distributed grains and particles. The microstructural effects were mainly attributed to the cavitation and streaming phenomena which took place during ultrasonic treatment in the melt. Tensile strength of the alloy was significantly improved by ultrasonic treatment of the melt. Discontinuity and refinement of $Mg_{17}Al_{12}$ particles in the ultrasonically treated samples is thought to be the main reason for this improvement. The paper also examines different possible mechanisms responsible for microstructural modification of different phases under ultrasonic treatment conditions.

1. Introduction

Considerable achievements have been made in the last few decades in developing various light alloys for production of metallic parts and assemblies in many diverse fields from automotive sector to oil industries and aerospace technologies. The requirements imposed on the quality of such products call for constant improvements in the metal processing technologies and above all in melting and casting practices.

Magnesium alloys have been widely used in the above mentioned applications due to their interesting combination of engineering properties such as low density, high specific strength and stiffness, improved damping property, electromagnetic shield capacity, excellent machinability and good castability [1].

AZ91 alloy is the most commonly used magnesium alloy. However, it has a high susceptibility to such solidification defects as hot tearing and microporosity. Different researches have shown that these defects can be overcome by refining the microstructures of the cast components [1,2]. Grain refinement is routinely practiced in casting industries and has a decisive effect on the structure and properties of castings and ingots. It can be carried out through many different methods, the most familiar of which is inoculation [3,4]. Electromagnetic vibration technique has also been successfully employed for modification of grain size and the grain size distribution of AZ91 alloy [5].

Another effective but less practiced method of grain refinement is ultrasonic treatment (UST). UST is a dynamic nucleation method in which ultrasonic vibrations (waves with frequencies equal to or higher than 20 kHz) are directed to the surface of a molten or solidifying alloy [6].

The idea of improving the quality of cast alloys by means of elastic oscillations produced by mechanical vibration or shaking applied to solidifying steel was first suggested by Chernov in 1878 [6]. However, the first experimentally observed effect of ultrasound on the solidification of molten metals generally dates back to 1936 when Socolov reported his experiments with sonication of molten zinc, tin and aluminium [6]. Detailed reviews of ultrasonic and vibration treatments of metals can be found in a paper by Campbell [7] and books by Eskin [6] and Abramov [8,9].

Effects of UST on refining the cast microstructure and removal of gasses and oxides from the melt have been associated with occurrence of acoustic cavitation and streaming in the liquid metal at certain sonication intensities [6]. During UST, when the melt is subjected to local random compression–expansion (tension) cycles, if the local pressure in the melt becomes less than its vapor pressure during the half-period of expansion, a cavity is formed. The cavity continues to grow until it collapses during the half-period

* Corresponding author. Fax: +98 311 3912752.
E-mail addresses: mohsenmse@ma.iut.ac.ir (M. Khosro Aghayani), behzn@cc.iut.ac.ir (B. Niroumand).

0925-8388/$ – see front matter © 2010 Elsevier B.V. All rights reserved.
doi:10.1016/j.jallcom.2010.08.139

of compression, thus producing a high intensity shock wave in the melt. Constant formation and collapse of thousands of such cavities create powerful waves that cycle into the melt [6,8].

It has been shown that the induced cavitation enables one to radically change the kinetics of crystallization and obtain extremely fine grains comparable in size to the cross section of a dendritic branch. This can improve plasticity in the cast and homogenized states without loss of strength [6,10–12].

Eskin investigated the effects of UST in the liquid pool of continuously cast aluminium ingots on inoculation potency of uncontrolled solid inclusions and modifying additions existing in the melt [6]. He concluded that in the absence of UST, only intrinsically active particles and modifiers took part in the nucleation, but with UST, even particles with large wetting angles (unwanted solid inclusions) were activated and contributed to nucleation, resulting in much smaller grains. In one case, for instance, he reported that the number of so-called activated "plankton" particles per cubic centimetre of the melt increased from 10^3 to 10^9 by UST. Such results showed that the effect of UST on the solidification microstructure was more than that of the cooling rate of the melt [6].

Zhang et al. [12] studied the effects of high-energy ultrasonic field on the microstructure and mechanical properties of A356 alloy. Their results indicated that the long dendritic silicon phases were broken into pieces and a considerable improvement in the mechanical properties were achieved by UST. Yu et al. [13] also reported considerable improvements in hardness, tensile strength and wear resistance of an Al–23%Si alloy by UST.

Zhong et al. [14] investigated the effects of ultrasonic vibration on iron-containing intermetallic compounds of two high silicon aluminium alloys. They found that UST not only refined the needle-like β-Al_5FeSi and plate-like δ-Al_4FeSi_2 intermetallic phases, but it encouraged the formation of δ phases more than β phases as well. They associated the latter observation with the effects of UST on more uniform distribution of iron atoms ahead of the solidification front and with the decrease in the formation temperature of the β phase. They also argued that more uniform distribution of solute in the melt restrained the rapid growth of δ phase in a single direction, causing the refinement of δ phase.

Zhang et al. [15] used a combination of UST and electromagnetic treatment to modify the microstructure of A356 alloy. They showed that the collective effects of ultrasonic cavitation, acoustic streaming and electromagnetic stirring resulted in significant refinement and spherodization of primary aluminium dendrites as well as the refinement of size and morphology of the eutectic silicon.

Li et al. [16] studied the effect of UST on the microstructure and refining ability of Al–5Ti–0.25C grain refining alloy. They showed that the morphology of $TiAl_3$ and TiC phases in the grain refining alloy was changed remarkably by UST, and $TiAl_3$ particles were refined due to such ultrasonic effects as cavitation and acoustic streaming. Furthermore, UST led to more effective dispersion of TiC particles in the aluminium matrix, enhanced the nucleation activity of TiC particles, and improved the refining effect of the grain refiner on an A1075 aluminium alloy.

More recently, Atamanenko et al. [17] investigated the effects of UST on grain refinement of some Zr and Ti containing aluminium alloys and formulated some criteria for efficient grain refinement of aluminium alloys by UST. They concluded that the efficiency of UST is significantly increased provided that aluminium alloys contain some zirconium with small additions (≥0.015 wt.%) of titanium, that UST is performed in the temperature range of primary solidification of Al_3Zr, and that the amplitude of vibrations is high enough to promote cavitation in the melt, *e.g.*, 20 μm.

An important point to note is that there are not as many published researches on UST of magnesium alloys as on aluminium alloys. Also, lack of similar criteria as those listed by Atamanenko et al. [17] for magnesium alloys is prevalent in the researches available. Nevertheless, there have been a number of investigations on the effects of UST on the microstructure and mechanical properties of magnesium alloys in recent years.

Liu et al. [18] and Gao et al. [19] studied the effect of ultrasonic power on the microstructure and mechanical properties of AZ91 magnesium alloy. These investigations showed that UST resulted in formation of fine non-dendritic grains in the solidified microstructures. According to these researchers, the acoustic cavitation and ultrasonically induced streaming in the melt, activation of insoluble impurity particles as nucleation centres, decrease in the temperature of the cavity/melt interfaces during the growth stage of the cavities, and faster cooling of the melt due to the ultrasonic streaming are the main factors that contribute to the refinement of the cast microstructures under UST. These investigations also showed that the tensile and compressive strengths as well as the fracture strains of the castings were improved by UST.

Ramirez et al. [20] and Qian et al. [21] studied the potency of UST for grain refinement of magnesium alloys and the effect of solute elements on its efficiency. Their interesting results indicated that UST could lead to a significant refinement only in the presence of adequate solute elements and that increasing the solute content at a low applied ultrasonic power level above the cavitation threshold was more effective than substantially increasing the applied ultrasonic power. They argued that the primary role of UST appeared to produce the initial crystallites by enhancing the nucleation and activating potential nucleation sites in the effectively irradiated melt volume.

Almost all the researches carried out on UST of magnesium alloys have only reported the influence of UST on the structural characteristics of the primary α-Mg, and very little information is available on the effects of UST on the intermetallic phases formed during solidification of magnesium alloys. For aluminium and silicon containing magnesium alloys, these phases may include Mg_2Si, MnFeAl(Si) and $Mg_{17}Al_{12}$ phases [22,23].

Zhiqiang et al. [24,25] investigated the effects of UST on the microstructure and mechanical properties of Mg–9.0 wt.%Al binary and AZ80 magnesium alloys and reported the effects of UST on the size and morphology of $Mg_{17}Al_{12}$ phase. They showed that $Mg_{17}Al_{12}$ phase in the entire cross section of the castings was significantly refined and also lost its continuity along the grain boundaries.

Lan et al. [26] used UST for dispersion of nano-sized SiC particles in molten AZ91D magnesium alloy to produce metal matrix nanocomposites. They showed a nearly uniform distribution and good dispersion of SiC nano-particles within the matrix. Although some agglomerates were found in the matrix, the particle agglomeration was greatly reduced when compared with the severe agglomeration in composites fabricated by traditional mechanical stirring method. They postulated that the strong cavitation impact coupled with local high temperature transients may break up the agglomerates and re-disperse the particles in the melt and at the same time significantly enhance the wettability between the solid particles and the melt.

The main mechanisms put forward in the literature to explain the role of cavitation in grain refinement of metals and alloys under UST can be classified as follows [6–9,12–21,24–27]:

(1) Cavitation produces temporarily localized high pressure points in the melt. According to the Clausius–Clapeyron equation, such an increase in the local pressures will increase the melting point of most alloys and, if used consciously, may render large localized undercoolings in the melt which results in intensified nucleation.
(2) Cavitation cleans the surface of the particles that are poorly wetted by the melt, thereby enhancing heterogeneous nucleation.

Table 1
Standard [17] as well as measured composition and liquidus temperature of AZ91 magnesium alloy used in this study.

Element	Al	Zn	Mn	Si	Cu	Ni	Mg	Liquidus
Standard	8.3–9.7%	0.35–1%	>0.13%	<0.5%	<0.1%	<0.03%	Bal.	595 °C
Used	9.3%	0.79%	0.33%	0.04%	0.005%	–	Bal.	598 °C

(3) Collapse of produced bubbles during their half-period of compression is accompanied by generation of pressure pulses as large as 100–1000 MPa. Such pulses can result in breaking of large grains and dendritic branches or disintegration of agglomerated inoculation substrates.
(4) Decreasing the local pressure in the produced bubbles in half-period of expansion results in vaporization of the melt from surface of the bubbles. Vaporization, being an endothermic phenomenon, decreases the surface temperature of the bubbles and may assist the nucleation of solid particles on these surfaces. These particles are distributed in the melt as soon as the bubbles collapse.
(5) At high ultrasonic intensity, the phenomenon of streaming becomes significant resulting in the development of mechanical pressure in the melt that may fragment the dendrite arms or disintegrate the agglomerated inoculation surfaces.
(6) Local melting of the roots of the dendrite arms due to increase in the local temperature of the melt in half-period of compression results in their separation from the mother dendrite. The separated particles will grow and form a new grain.

As one may notice, some of these mechanisms are effective above and some below the liquidus temperature of an alloy and also many of them may occur simultaneously.

This paper presents the results of a study on the effects of UST on the microstructural features of AZ91 magnesium alloy. Also, special attention is paid to the effects of UST on the intermetallic phases formed in the microstructures. This is an area less explored by other researchers.

2. Materials and methods

The standard [28] as well as measured composition and liquidus temperature of AZ91 magnesium alloy used in this study are shown in Table 1. In each experiment, about 320 g of the alloy was melted in an electrical muffle furnace. The alloy was heated to 700 °C where it was isothermally subjected to continuous sonication for 5 min and was then poured into a sodium-silicate bonded sand mould. A sand mould rather than a metallic die was employed in this research to reduce the effects of cooling rate on microstructural refinement of the alloy. The surface of the melt was covered by MAGREX flux (Foseco Foundry International Limited) during the melting and holding period to protect it from the atmosphere and prevent its oxidation.

Fig. 1 displays the ultrasonic oscillation device used in this study. It consisted of an acoustic generator and transducer with a maximum power of 600 W and fixed frequency of about 20 kHz, a water cooled horn, and a movable platform. In each experiment, as soon as the melt temperature was stabilized at 700 °C, the device was lowered and 5 mm of the tip of its horn was immersed into the melt. The molten alloy was then treated for 5 min at an ultrasonic intensity corresponding to 0, 20, 40 or 60% of the nominal maximum power of the device. The first sample was treated under the same conditions with the horn in contact with the melt but without UST.

The cast samples were then sectioned, ground, polished and etched with 2% Nital solution [29]. Microstructural features of the cast samples were identified using energy dispersive spectrophotometric (EDS) analysis and characterized employing standard optical microscopy techniques and Clemex image analysis software [30]. For each sample, the average equivalent circle diameter and the sphericity of the grains and the intermetallic phases, i.e., Mg_2Si, MnFeAl(Si) and $Mg_{17}Al_{12}$ particles, were calculated. For $Mg_{17}Al_{12}$ particles, the average length and width of the particles were also measured. The equivalent circle diameter and the sphericity of each microstructural feature were calculated using Eqs. (1) and (2), respectively. As calculated sphericity value increases, the particles become more globular:

$$d = \sqrt{\frac{4 \times \text{area}}{\pi}} \tag{1}$$

$$\text{Sphericity} = \frac{4 \times \pi \times \text{area}}{(\text{perimeter})^2} \tag{2}$$

"Standard error of the mean", α, for the measurements, which will be shown as error bars in the curves, was calculated using Eq. (3) where n and σ indicated the number and the standard deviation of the measurements, respectively. σ was calculated from Eq. (4) where $\bar{X}$ and x represented the mean quantity of total samples and quantity of each sample, respectively [31].

$$\alpha = \frac{\sigma}{\sqrt{n}} \tag{3}$$

$$\sigma = \sqrt{\sum \frac{(x - \bar{x})^2}{n-1}} \tag{4}$$

Tensile test specimens were prepared in conformance with ASTM E8 standard from each sample and were tested using a Hounsfield tensile tester machine. "Standard error of the mean" for the tensile strengths was calculated using Eq. (3).

3. Results and discussion

3.1. Effects of UST power on α-Mg grains

Fig. 2 shows the microstructures of AZ91 alloy without UST and with UST for 5 min with different applied UST power levels. Microstructures of all samples show equiaxed dendrites of primary α-Mg phase. However, the dendrites are coarser and less uniform in the sample without UST. Although magnesium alloys with high aluminium content are generally fine grained, Fig. 2 reveals that increasing the applied UST power has continuously reduced the grain size and increased the uniformity of the grains.

Fig. 3 illustrates the effect of applied UST power on the equivalent circle diameter of the grains. It is evident that even low power UST has significantly reduced the grain size. The figure shows that the equivalent circle diameter of the dendrites has dropped from about 280 μm to about 125 μm by increasing the applied UST power.

Effect of applied UST power on the grains sphericity is demonstrated in Fig. 4 where it is shown that the sphericity of grains is increased by increasing the UST power. Of course, since grains are still dendritic, their sphericity is far from unity, but as it can be seen from Fig. 2, they have less branches and shorter arms, which result in smaller grain perimeters and greater sphericity (Eq. (2)). Figs. 3 and 4 also demonstrate that the uniformity of the grains

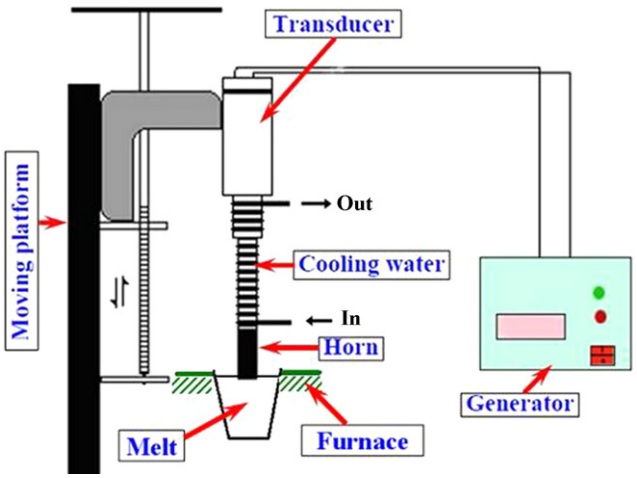

Fig. 1. Schematic of the ultrasonic treatment set-up used in this study.

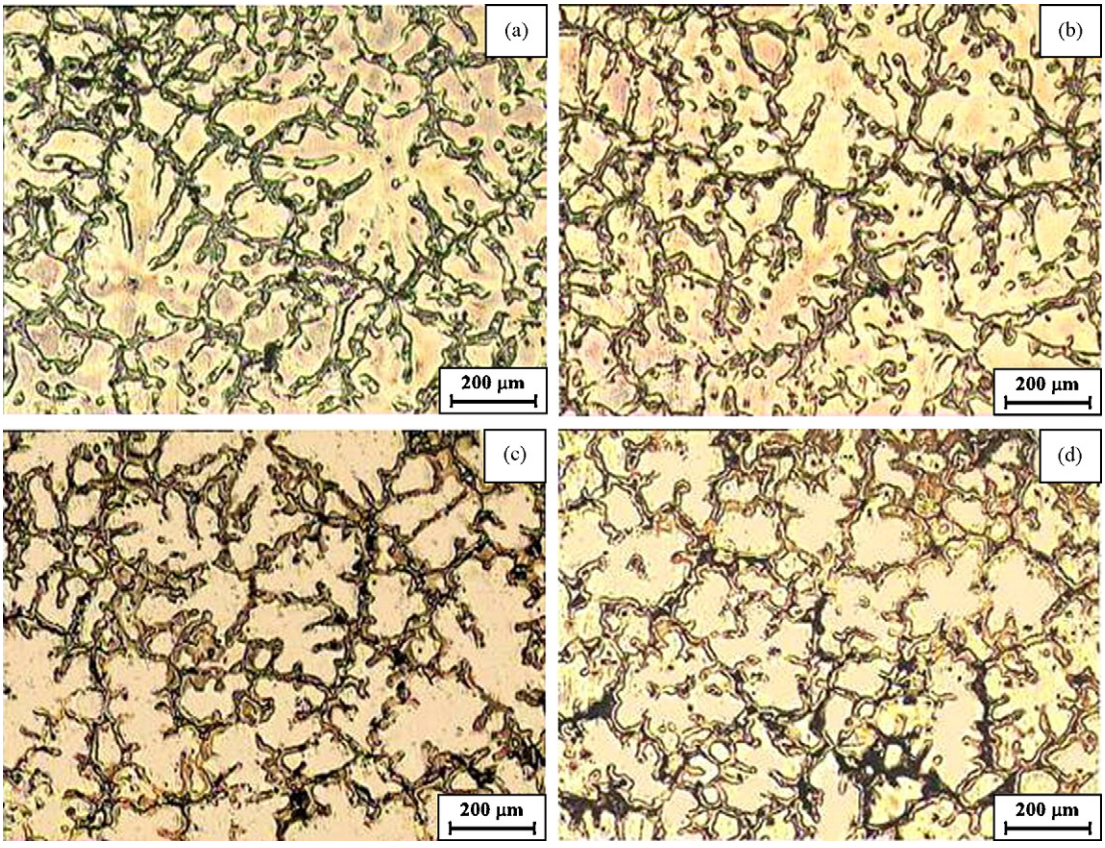

Fig. 2. Microstructures of AZ91 alloy cast at 700 °C: (a) without UST, and with UST for 5 min at (b) 20%, (c) 40% and (d) 60% applied power.

in terms of their size and shape has increased by increasing the applied UST power.

Different mechanisms proposed for the microstructure refining effects of UST were summarized in the introduction section. In this study, UST was performed at about 102 °C above the measured liquidus temperature of the alloy. No α-Mg grain is expected to form at this temperature, and therefore the fragmentation effect of cavitation and streaming phenomena is not expected to be a contributing factor to the microstructural refinement. However, it has been shown [6] that cavitation may generate localized pressure pulses of the order of 100–1000 MPa. A simple calculation using Clausius–Clapeyron equation and thermo-physical properties of molten magnesium shows that the melting point of the alloy can increase between 12 and 120 °C under such pressures. Therefore, if the local pressure in some parts of the melt is randomly increased to about 850–1000 MPa during UST, the local melting point of the alloy can increase to about 102–120 °C, which results in sudden local undercoolings of the order of 0–18 °C at these points. Under such conditions, nucleation and growth of some α-Mg particles may become possible. However, the condition is a transient one and the solid particles formed are not expected to survive after the local pressure has reduced again or during the interval between the cessation of UST and pouring of the melt in the mould. As a result, fragmentation of solid α-Mg dendrites or formation of high undercoolings in the melt under UST does not appear to be a major contributing factor to the refinement of the α-Mg grains.

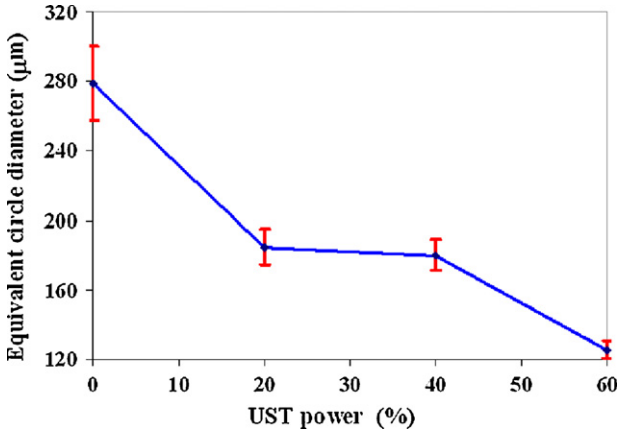

Fig. 3. Effect of applied ultrasonic power on equivalent circle diameter of α-Mg grains.

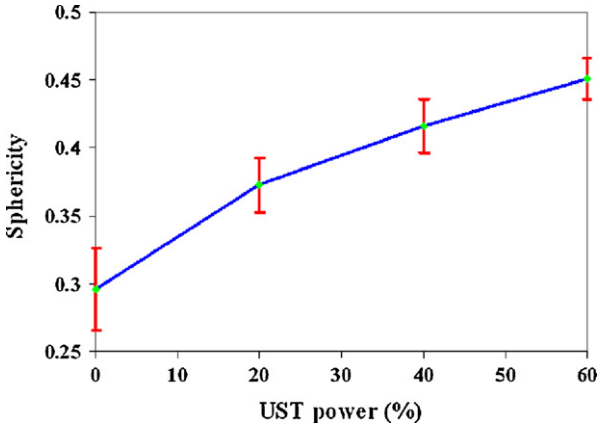

Fig. 4. Effect of applied ultrasonic power on sphericity of α-Mg grains.

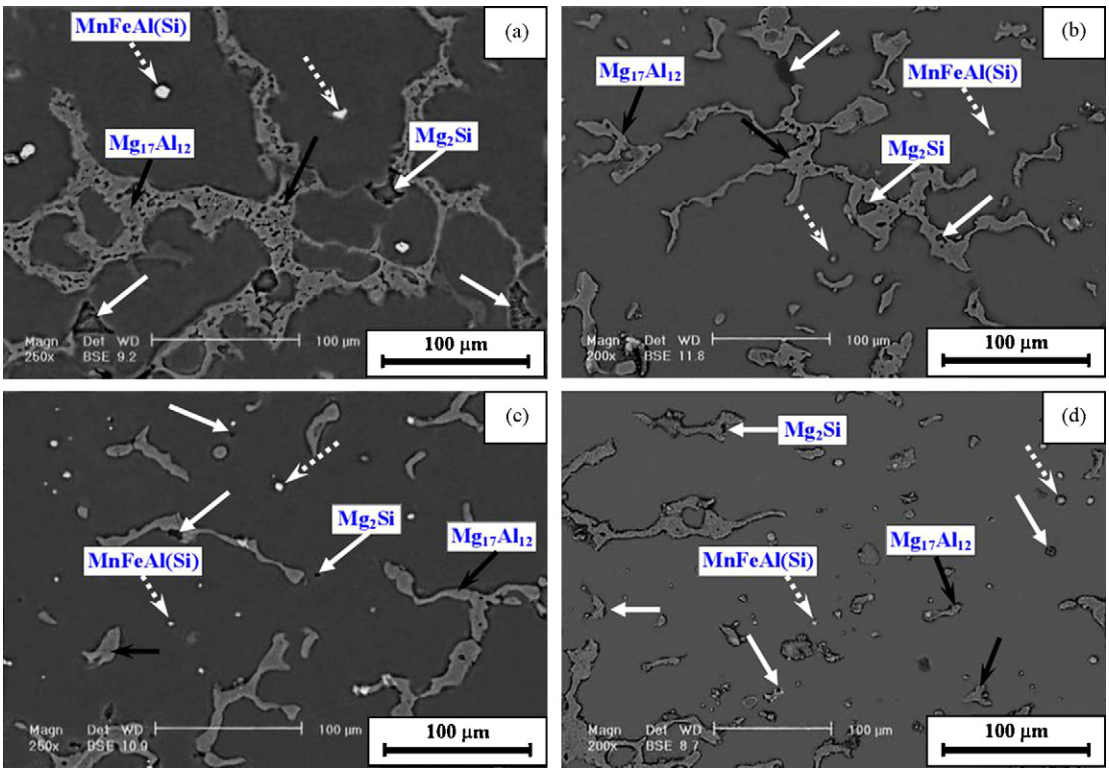

Fig. 5. SEM micrographs of different intermetallic phases observed in different samples: (a) without UST, and with UST for 5 min at (b) 20%, (c) 40% and (d) 60% applied power.

Therefore, under the experimental conditions employed in this study, the changes brought about by UST in the microstructure of α-Mg dendrites is thought to be mostly related to the effects of ultrasonic cavitation on cleaning the surfaces of the poorly wetted particles in the melt thereby enhancing their nucleation potency. Furthermore, disintegration and distribution of the agglomerated nucleant particles existing in the melt under the effects of cavitation and streaming also increases the effective nucleation sites.

Increased density of the active nuclei in the melt results in earlier hard as well as soft impingement of the grains [32]. In other words, not only is the radial growth of each individual grain stopped earlier by coming into contact with the neighbouring grains (hard impingement), but overlap of the thermal and solutal fields of the neighbouring grains (soft impingement) happens more rapidly as well. The latter tends to decrease the instability of the solid-liquid interfaces of the growing grains, and therefore prohibit the formation of new branches and arms. These effects will render smaller and more rounded grains with smaller number of dendrite arms, as can be observed from Figs. 2–4.

3.2. Effects of UST power on intermetallic phases

Scanning electron microscopic (SEM) micrographs of different samples are shown in Fig. 5. Three types of intermetallics could be detected in the cast microstructures of AZ91 alloy based on their shapes and morphology. They included an angular, a relatively spherical and an elongated phase, whose typical SEM images are shown in Fig. 6 at higher magnifications. Table 2 presents the results of EDS analysis of the particles marked in Fig. 6. The results identifies the intermetallics to be in the order of Mg_2Si, MnFeAl(Si) and $Mg_{17}Al_{12}$.

As can be clearly seen from Fig. 5, the dominant intermetallic phase in the microstructures is $Mg_{17}Al_{12}$. Considering the chemical composition of the alloy, the other two intermetallic phases are by far less abundant than $Mg_{17}Al_{12}$, but still present in detectable quantities. It is somewhat surprising that while the occurrence of MnFeAl(Si) in AZ91 alloy has been widely reported [1,22], iron limits for AZ91 alloy are not indicated in many references [28], and consequently at least some optical emission spectrometry systems are not programmed to record iron concentration in the alloy. As a result, while Table 1 does not show the iron content of the alloy, EDS analyses prove the existence of MnFeAl(Si) phase in the microstructures.

The dominant intermetallic phase in the microstructures, i.e., $Mg_{17}Al_{12}$, is formed by an eutectic reaction in the Mg-Al system at about 42.8–43.4 at.% Al content and 437 °C [23]. Due to its low formation temperature, $Mg_{17}Al_{12}$ is the last solid phase formed during solidification, and therefore, as can be seen from Figs. 5 and 6(c), it precipitates at the grain boundaries. Being a brittle phase [1], $Mg_{17}Al_{12}$ can have deleterious effects on the mechanical proper-

Table 2
Results of energy dispersive spectrophotometric (EDS) analysis of different phases shown in Fig. 6.

Phase	Normalized comp.			Intermetallic type
	Element	Weight%	Atomic%	
(a)	Mg	60.98	64.31	Mg_2Si
	Al	2.12	2.01	
	Si	36.90	33.68	
(b)	Mg	1.19	1.92	MnFeAl(Si)
	Al	35.52	51.78	
	Si	1.62	2.27	
	Mn	50.14	35.90	
	Fe	11.54	8.13	
(c)	Mg	57.65	62.01	$Mg_{17}Al_{12}$
	Al	37.00	35.85	
	Zn	5.34	2.14	

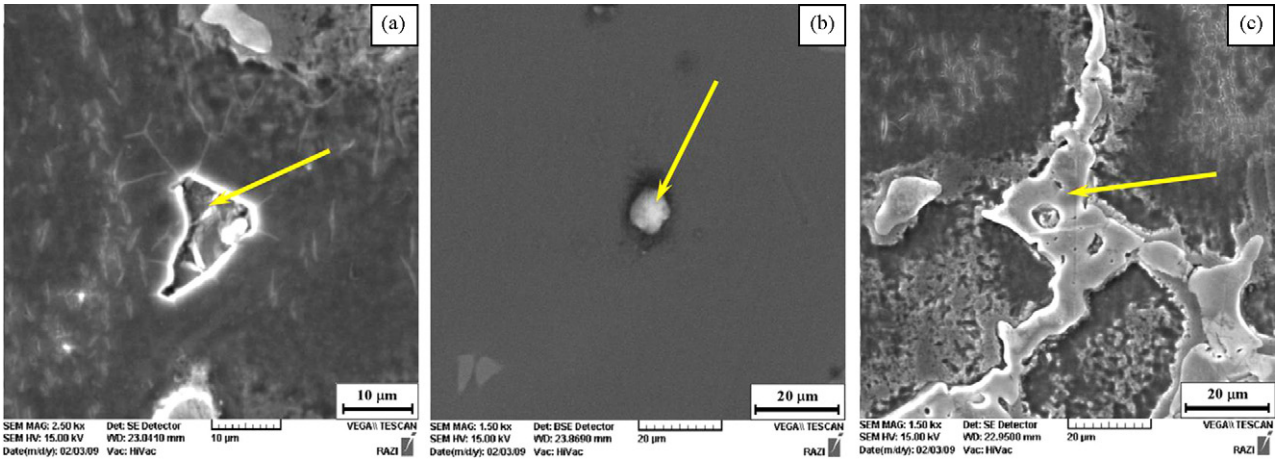

Fig. 6. SEM micrographs of (a) Mg_2Si, (b) MnFeAl(Si), and (c) $Mg_{17}Al_{12}$ phases.

ties of the castings if it forms a continuous network at the grain boundaries.

Fig. 5 demonstrates that under UST, the continuity and thickness of $Mg_{17}Al_{12}$ particles are decreased. Effects of applied UST power on the average equivalent circle diameter, length and width of $Mg_{17}Al_{12}$ particles are shown in Fig. 7. Effects of applied UST power on average sphericity as well as on the distribution of sphericity values of $Mg_{17}Al_{12}$ particles are presented in Fig. 8. The results presented in Figs. 7 and 8 were measured from about 130 to 360 $Mg_{17}Al_{12}$ particles in different samples, where the lower limit corresponded to the sample cast without UST.

Figs. 7 and 8 indicate that the size of $Mg_{17}Al_{12}$ particles decreases and their sphericity increases by increasing the applied UST power. Even low power UST has significantly reduced the size of the particles and improved their uniformity and distribution. Fig. 7b shows that the average length of $Mg_{17}Al_{12}$ particles has reduced from 95 μm without UST to 33 μm at the highest applied UST power level. This renders diminished continuity of $Mg_{17}Al_{12}$ particles as shown in Fig. 5(d).

Fig. 8 reveals that while the sphericity of all $Mg_{17}Al_{12}$ particles in the microstructure of the sample cast without UST is below 0.6, UST has increased the sphericity of these particles, and at the highest applied UST power level, a considerable number of $Mg_{17}Al_{12}$ particles with sphericity values between 0.8 and 1.0 have appeared.

Mg_2Si, magnesium silicide, is a stoichiometric intermetallic compound and the only stable compound in the Mg–Si system. It has a melting point of 1085 °C [23]. Maximum solid solubility of Si in Mg is 0.003 at.%. There are two eutectic reactions in Mg–Si system:

(1) $L \rightarrow (Mg) + Mg_2Si$
(2) $L \rightarrow (Si) + Mg_2Si$

The composition and temperature of the eutectic point between Mg and Mg_2Si on Mg-rich side are 1.16 at.%Si and 637 °C, respectively [23]. Therefore, for the alloy used in this study, Mg_2Si particles are expected to form at the eutectic temperature of about 637 °C.

Remarkable changes in the size and shape of Mg_2Si particles with UST are shown in Fig. 5. The figure shows that with UST at 60% of maximum power, Mg_2Si particles have transformed to globular and finer particles. Effects of applied UST power on the average equivalent diameter, sphericity and distribution of sphericity values of Mg_2Si particles are shown in Figs. 9 and 10, respectively. The results presented in the figures for Mg_2Si particles were measured

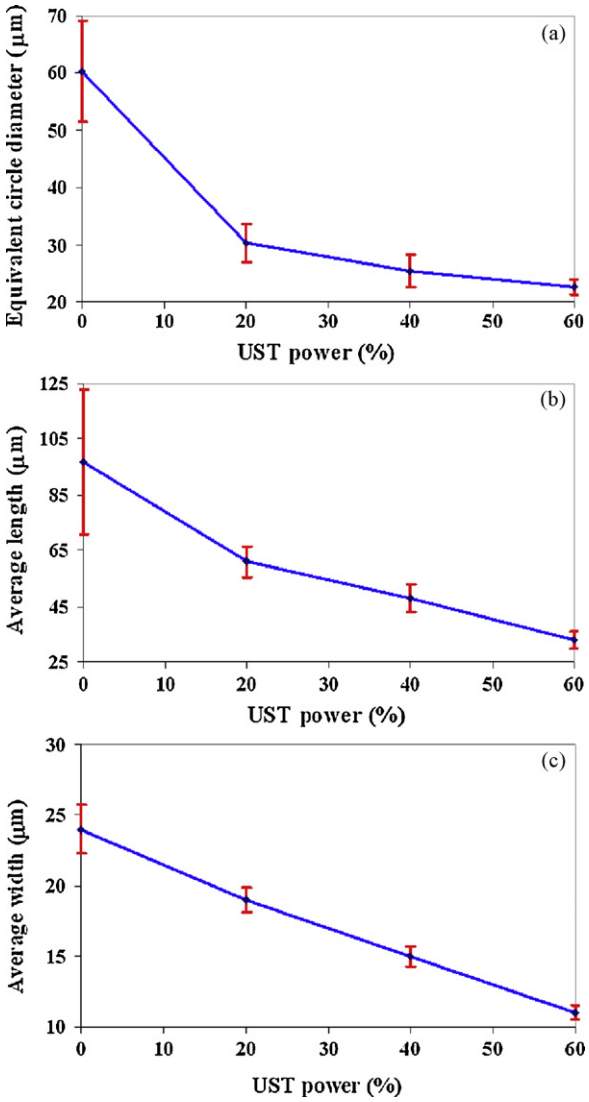

Fig. 7. Effect of applied ultrasonic power on (a) equivalent circle diameter, (b) average length, and (c) average width of $Mg_{17}Al_{12}$ particles.

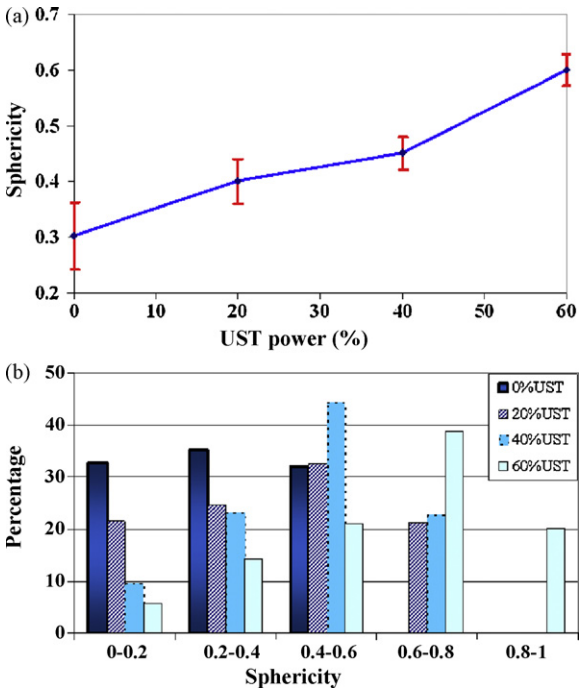

Fig. 8. Effect of applied ultrasonic power on (a) sphericity and (b) distribution of sphericity values of $Mg_{17}Al_{12}$ particles.

from about 30 to 140 particles in different samples where the lower limit corresponded to the sample cast without UST.

Figs. 9 and 10 reveal a decreasing trend for Mg_2Si particle size and an increasing trend for their sphericity by increasing the applied UST power. Application of 60% of maximum power has produced the most refined particles where all Mg_2Si particles have sphericity values between 0.8 and 1.0.

Figs. 5, 9 and 10 also show the effect of UST on size, sphericity and sphericity distribution of MnFeAl(Si) particles, which form at about 650 °C [22], and reveal that similar to the previous phase, the average size of MnFeAl(Si) particles decreases and their sphericity increases by increasing the applied UST power. Of course, since MnFeAl(Si) particles are intrinsically round, the effect of UST on the sphericity of this phase is not as significant as on that of previous phases. The results presented in Figs. 9 and 10 for MnFeAl(Si) particles were measured from about 40 to 110 particles in different samples where the lower limit corresponded to the sample cast without UST.

It seems that the mechanisms through which UST affects the size and shape of different intermetallic phases formed during solidification of AZ91 alloy depend on the temperature range during

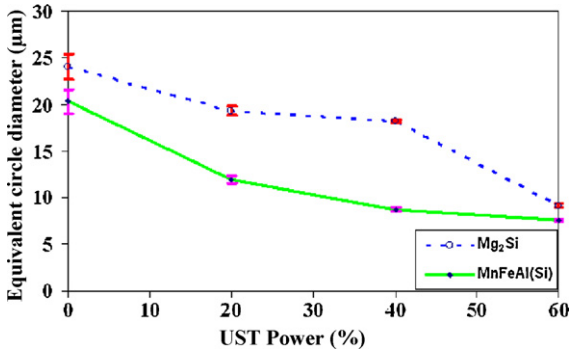

Fig. 9. Effect of applied ultrasonic power on average equivalent diameter of Mg_2Si and MnFeAl(Si) particles.

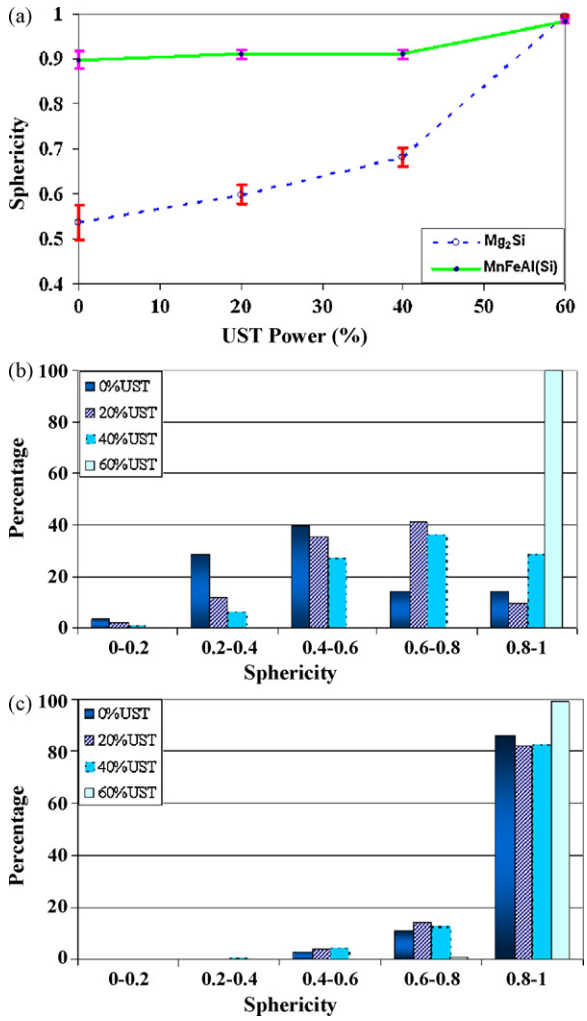

Fig. 10. Effect of applied ultrasonic power on (a) sphericity of Mg_2Si and MnFeAl(Si) particles, (b) distribution of sphericity values of Mg_2Si particles, and (c) distribution of sphericity values of MnFeAl(Si) particles.

cooling where they are formed. Mg_2Si is formed at about 637 °C in alloys containing less than 0.5%Si [23] and the formation temperature of MnFeAl(Si) is about 650 °C [22]. Therefore, both of these phases are formed at temperatures less than but relatively close to the UST temperature. On the other hand, the formation temperature of $Mg_{17}Al_{12}$ is about 437 °C [23] which is much lower than the UST temperature. These differences must be taken into account when the mechanisms governing the effect of UST on different phases are investigated.

An account of different mechanisms that may be responsible for the changes brought about by UST in the intermetallic phases is presented below. As will be seen, some of the mechanisms are effective for all the three intermetallic phases and some are only affective for certain intermetallic phases.

1. One of the main mechanisms governing the changes in the shape and size of intermetallic phases is indeed the cavitation phenomenon which cleans the surfaces of the foreign particles in the melt and improves their wettability by the melt, therefore increasing the heterogeneous nucleation of the intermetallic phases. This seems to be a general mechanism effective in all the three intermetallic phases.
2. Another effective mechanism for all the three intermetallic phases is the disintegration and distribution of the agglomerated nucleant particles existing in the melt under the effects of cav-

itation and streaming which increases the effective nucleation sites.

3. Decrease in the surface temperature of the bubbles in their half-period of expansion because of vaporization of melt from bubble surface is another possible mechanism for microstructural refinement under UST. If the surface temperature drops to the extent that the intermetallic phases can nucleate on the surfaces of bubbles, collapse of bubbles results in finer grains and more uniform distribution of the intermetallic phases.
4. Another phenomenon is the possibility of occurrence of sudden high local undercoolings in the melt due to the change in the melting point of the intermetallic phases by increasing the local pressures according to Clausius–Clapeyron equation. Creation of such undercoolings depends on the extent of changes in the melting temperature of the intermetallic phases as well as the distance between the actual temperature of the melt and the formation temperature of the phases without UST. The smaller this distance, the more significant the influence of UST. Therefore, the effect of this mechanism on refinement of Mg_2Si and MnFeAl(Si) phases whose formation temperatures are only about 50–60 °C less than the UST temperature appears to be significant. However, for $Mg_{17}Al_{12}$ phase whose formation temperature is about 260 °C less than the UST temperature, the effect of this mechanism must be negligible.
5. Following the preceding effect, the Mg_2Si and MnFeAl(Si) particles formed due to creation of sudden undercooling conditions in the melt may be fragmented under the influence of mechanical forces generated by bubble collapse or streaming phenomenon and still becomes finer and better distributed. For $Mg_{17}Al_{12}$, such an effect does not seem to be likely.
6. When the local temperature of the melt is increased in half-period of compression of bubbles, thinner parts and sharp edges of the Mg_2Si and MnFeAl(Si) phases that are likely to form at the UST temperature may suffer local melting. This not only increases the number of growing intermetallic particles but it can encourage their spheroidization as well (especially for Mg_2Si phase). This mechanism doesn't seem to be very effective for $Mg_{17}Al_{12}$ particles.
7. $Mg_{17}Al_{12}$ phase is formed at the last stages of solidification at the boundaries of primary α-Mg grains. In addition to other mechanisms affecting the nucleation density of $Mg_{17}Al_{12}$ particles, increased grain boundaries of primary α-Mg and improved uniformity of chemical composition of the melt under UST result in precipitation of this phase in more locations, thereby decreasing its continuity and size.
8. No matter by what mechanism the number of growing particles is increased, it results in earlier hard and soft impingement of the intermetallic particles with other intermetallic particles or primary α-Mg grains as discussed earlier. Furthermore, cavitation induced high speed flow in the melt also helps to reduce the concentration gradient around the growing particles and decreases the chance of formation of constitutional undercooling zone in front of the growing particles which can destabilize their interfaces. These effects tend to stabilize the solid–liquid interfaces of the growing particles and render more rounded particles as shown in Figs. 8 and 10.

3.3. Effects of UST power on tensile strength of AZ91 alloy

It was shown in the preceding sections that UST could bring about significant microstructural improvements in terms of size and shape of different metallic or intermetallic phases formed during solidification of AZ91 alloy. Tensile tests were conducted to study the effects of UST on tensile strength of the samples and investigate the connection between the microstructural improvement and the mechanical properties.

Table 3
Effect of applied UST power on tensile strength of AZ91 alloy.

	UST power			
	0%	20%	40%	60%
Tensile strength (MPa)	94 ± 2	139 ± 3	152 ± 5	165 ± 6

Table 3 shows the effect of UST power on the average tensile strength of AZ91 alloy. As depicted in the table, the tensile strength of the alloy has continuously increased by increasing the UST power from about 94 MPa for the sample cast without UST to about 165 MPa for the sample treated at 60% UST power.

More uniform and finer α-Mg dendrites as well as smaller and more spherical intermetallic phases present in the microstructure each contribute to some extent to the improvement of the tensile strength of the alloy as the applied UST power is increased.

More grain boundaries associated with finer α-Mg grains would obviously result in better mechanical properties. However, it is thought that discontinuity and refinement of $Mg_{17}Al_{12}$ particles should play a major role in improvement of the tensile strength of the alloy. In conventional AZ91 castings, $Mg_{17}Al_{12}$ constitutes a continuous brittle phase at the grain boundaries of α-Mg dendrites which controls the mechanical properties of the castings. The results presented in the previous sections showed that under UST, continuity, thickness and width of $Mg_{17}Al_{12}$ particles decreased and their sphericity increased. These alone would result in higher tensile strength of the alloy.

On the other hand, AZ91 can be considered a particulate metal matrix composite consisting of Mg_2Si and MnFeAl(Si) particles dispersed in an α-Mg matrix. Decrease in the size and increase in the number of Mg_2Si and MnFeAl(Si) particles distributed in the microstructure due to refinement effects of UST would result in the increased dislocation density in the matrix. This is due to the thermal expansion mismatch of the matrix and the reinforcement at the particles–matrix interfaces [33]. Spheroidization of these brittle phases further reduces the stress concentration sites in the microstructures.

It seems that the collective effects of UST on these microstructural features have significantly improved the tensile strength of AZ91 alloy as shown in Table 3.

4. Conclusions

In this study, the effects of ultrasonic treatment on microstructural features and tensile strength of AZ91 magnesium alloy were investigated. The results showed that ultrasonic treatment of the melt prior to casting had a significant effect on the size and sphericity of α-Mg dendrites as well as on the size, continuity, sphericity and distribution of intermetallic particles formed during cooling and solidification of the alloy. Increasing the applied ultrasonic power generally resulted in smaller, more rounded and better distributed grains and intermetallic particles. The microstructural effects were mainly attributed to the cavitation and streaming phenomena which took place during ultrasonic treatment in the melt. Different possible mechanisms responsible for microstructural modification of different phases under ultrasonic treatment conditions were also discussed. Tensile strength of the alloy was significantly improved by ultrasonic treatment of the melt. Discontinuity and refinement of $Mg_{17}Al_{12}$ particles in the ultrasonically treated samples is thought to be the main reason for this improvement.

References

[1] H.E. Friedrich, B.L. Mordike, Magnesium Technology (Metallurgy, Design Data, Applications), Springer, Berlin, 2006.

[2] X. Liu, Y. Osawa, S. Takamori, T. Mukai, Mater. Lett. 62 (2008) 2872–2875.
[3] Q. Jin, J.P. Eom, S.G. Lim, W.W. Park, B.S. You, Scripta Mater. 49 (2003) 1129–1132.
[4] P. Cao, D.H. StJohn, M. Qian, Mater. Sci. Forum 488–489 (2005) 139–142.
[5] M. Li, T. Tamura, N. Omura, K. Miwa, J. Alloys Compd. 494 (2010) 116–122.
[6] G.L. Eskin, Ultrasonic Treatment of Light Alloy Melts, Gordon and Breach, Amsterdam, 1998.
[7] J. Campbell, Int. Met. Rev. 26 (1981) 71–108.
[8] O.V. Abramov, High-Intensity Ultrasonics: Theory and Industrial Applications, CRC Press, 1999.
[9] O.V. Abramov, Ultrasound in Liquid and Solid Metals, CRC Press, London, 1994.
[10] Q. Liu, Q. Zhai, F. Qi, Y. Zhang, Mater. Lett. 61 (2007) 2422–2425.
[11] Q. Liu, Y. Zhang, Y. Song, F. Qi, Q. Zhai, Mater. Des. 28 (2007) 1949–1952.
[12] S. Zhang, Y. Zhao, X. Cheng, G. Chen, Q. Dai, J. Alloys Compd. 470 (2009) 168–172.
[13] S.R. Yu, H.K. Feng, Y.L. Li, L.Y. Gong, J. Alloys Compd. 484 (2009) 360–364.
[14] G. Zhong, S. Wu, H. Jiang, P. An, J. Alloys Compd. 492 (2010) 482–487.
[15] Z. Zhang, J. Li, H. Yue, J. Zhang, T. Li, J. Alloys Compd. 484 (2009) 458–462.
[16] Y.L. Li, H.K. Feng, F.R. Cao, Y.B. Chen, L.Y. Gong, Mater. Sci. Eng. A 487 (2008) 518–523.
[17] T.V. Atamanenko, D.G. Eskin, L. Zhang, L. Katgerman, Metall. Mater. Trans. A 41 (2010) 2056–2066.
[18] X. Liu, Y. Osawa, S. Takamori, T. Mukai, Mater. Sci. Eng. A 487 (2008) 120–123.
[19] D. Gao, Z. Li, Q. Han, Q. Zhai, Mater. Sci. Eng. A 502 (2009) 2–5.
[20] A. Ramirez, M. Qian, B. Davis, T. Wilks, D.H. StJohn, Scripta Mater. 59 (2008) 19–22.
[21] M. Qian, A. Ramirez, A. Das, D.H. StJohn, J. Cryst. Growth 312 (2010) 2267–2272.
[22] A. Ditze, C. SCharf, Recycling of Magnesium, Papierflieger Verlag GmbH, 2008.
[23] A.A. Nayeb-Hashemi, J.B. Clark, Phase Diagrams of Binary Magnesium Alloys, ASM International, 1988.
[24] Z. Zhiqiang, L. Qichi, C. Jianzhong, Rare Met. 28 (2009) 86–90.
[25] Z. Zhiqiang, L. Qichi, C. Jianzhong, Trans. Nonferr. Met. Soc. China 20 (2010) s376–s381.
[26] J. Lan, Y. Yang, X. Li, Mater. Sci. Eng. A 386 (2004) 284–290.
[27] X. Jian, The Effect of Ultrasonic Vibration on the Solidification of Light Alloys, Ph.D. dissertation, The University of Tennessee, 2005.
[28] ASM Handbook: Properties and Selection: Nonferrous Alloys and Special-Purpose Materials, vol. 2, 10th ed., ASM, 1993.
[29] ASM Handbook: Metallography and Microstructures, vol. 9, 9th ed., ASM, 1992.
[30] http://www.clemex.com/Products/ImageAnalysis/Software.aspx, last accessed on 25.12.2009.
[31] J. Topping, Errors of Observation and their Treatment, 4th ed., Chapman & Hall, 1972.
[32] W. Kurz, D.J. Fisher, Fundamentals of Solidification, 4th ed., Trans. Tech. Publication, Switzerland, 1998.
[33] K.K. Deng, K. Wu, Y.W. Wu, K.B. Nie, M.Y. Zheng, J. Alloys Compd. 504 (2010) 542–547.